Possible band termination in ^{99}Rh

M. Sugawara*
Chiba Institute of Technology, Narashino, Chiba 275-0023, Japan

T. Hayakawa, M. Oshima, Y. Toh, A. Osa, M. Matsuda, T. Shizuma, and Y. Hatsukawa
Japan Atomic Energy Agency, Tokai, Ibaraki 319-1195, Japan

H. Kusakari
Chiba University, Inage-ku, Chiba 263-8522, Japan

T. Morikawa
Kyushu University, Hakozaki, Fukuoka 812-8581, Japan

Z. G. Gan
Institute of Modern Physics, Chinese Academy of Science, Lanzhou 730000, P.R. China

T. Czosnyka
Heavy Ion Laboratory, Warsaw PL-02097, Poland
(Received 12 March 2013; revised manuscript received 30 May 2013; published 26 June 2013)

High-spin states of ^{99}Rh were studied through in-beam γ-ray spectroscopy by using the reaction ^{68}Zn(^{37}Cl, $\alpha 2n$). The upper part of the band based on the $g_{9/2}$ proton orbital was rearranged in four parallel cascades. Negative parity was tentatively assigned for the side-band that previously had no parity assignment. This negative-parity band was interpreted as having the configuration of $\pi(g_{9/2})^5\nu[(d_{5/2}g_{7/2})^3(h_{11/2})]$ and extended up to $\frac{51}{2}^{(-)}$, which is possibly a terminating state. The band based on the $p_{1/2}$ proton orbital was observed up to $\frac{29}{2}^-$ and its property was compared with those of neighboring odd-Z nuclei from the two different viewpoints, one of which is a weakly deformed soft rotor with spin alignments and the other is vibrational to rotational evolution along the band.

DOI: 10.1103/PhysRevC.87.064319 PACS number(s): 23.20.Lv, 21.10.Re, 27.60.+j, 21.60.−n

I. INTRODUCTION

Considered from a microscopic point of view, the total angular momentum of a nucleus is built from individual angular momenta of nucleons outside the closed shell (valence nucleons). In a rotating nucleus individual angular momenta of more and more valence nucleons align to the rotational axis due to Coriolis and centrifugal forces with increasing spin. Consequently, the rotational band for a given configuration ceases to exist at its maximum spin value, which is called band termination.

The phenomenon of band termination was extensively studied in the last two decades [1]. Good examples are in the neutron-deficient region close to the doubly magic ^{100}Sn, where terminating configurations have been observed over their entire spin range [2,3]. Band termination has been analyzed theoretically mainly based on the configuration-dependent cranked Nilsson-Strutinsky approach [1]. In this formalism the configurations are determined by the number of particles in the N shells of the rotating basis. Additionally particles in the intruder high-j shells can be distinguished from ones in the other j shells. The different configurations are then labeled by the number of particles in the different j shells relative to a ^{90}Zr core. Since relevant high-j orbitals for band termination in this region are $\pi g_{9/2}$ and $\nu h_{11/2}$, the shorthand notation $[p, n]$ is usually used, where p is the number of protons in $g_{9/2}$ orbitals, and n the number of neutrons in $h_{11/2}$ orbitals. Terminating states for the [4, 1] and [5, 1] configurations have been observed in ^{98,99,100}Ru [4] and ^{101}Rh [5], respectively. However an analogous state has not yet been observed so far in ^{99}Rh.

Another interesting aspect of ^{99}Rh concerns the position of the $\pi p_{1/2}$ orbital relative to that of $\pi g_{9/2}$. As for the $N = 54$ isotones, the spin-parity of the ground state is $\frac{1}{2}^-$ in ^{99}Rh, while it is $\frac{9}{2}^+$ in ^{97}Tc and ^{101}Ag. Therefore it is more likely in ^{99}Rh than in the other isotones that we can observe the higher-spin members of the rotational band based on the $\pi p_{1/2}$ orbital.

Prior to this work, there have been several γ-ray spectroscopic studies of ^{99}Rh. Detailed knowledge of low-spin states has been obtained by studying γ transitions following the electron capture decay of ^{99}Pd and the ^{99}Ru(p,n) reaction [6,7]. High-spin states have been investigated via ^{16}O-induced reactions, and two bands based on $\pi p_{1/2}$ and $\pi g_{9/2}$ orbitals have been observed [8]. It was claimed more than ten years ago that the band based on the $\pi g_{9/2}$ orbital was observed to the $\frac{49}{2}^+$ state in the study using the ^{66}Zn(^{37}Cl, $2p2n$) reaction [9].

This paper is organized as follows. First, we describe the experimental methods and results in Sec. II. The discussion in

*masahiko.sugawara@it-chiba.ac.jp

TABLE I. Properties of γ rays observed in this experiment. Relative intensities are normalized to that of the 778-keV transition from $\frac{13}{2}^+$ to $\frac{9}{2}^+$. ADO ratios are tabulated for different combinations of detectors.

$I_i \rightarrow I_f$	E_γ (keV)	I_γ	ADO (32°/90°)	ADO (58°/90°)	Multipolarity
Band "$p_{1/2}$"					
$\frac{5}{2}^- \rightarrow \frac{1}{2}^-$	427.3(1)	6.0(4)			
$\frac{9}{2}^- \rightarrow \frac{5}{2}^-$	552.3(1)	5.9(4)	1.28(6)	1.21(6)	Quadrupole
$\frac{13}{2}^- \rightarrow \frac{9}{2}^-$	681.3(1)	5.6(3)	1.43(7)	1.39(7)	Quadrupole
$\frac{17}{2}^- \rightarrow \frac{13}{2}^-$	640.0(1)	5.5(3)	1.45(8)	1.18(7)	Quadrupole
$\frac{21}{2}^- \rightarrow \frac{17}{2}^-$	813.1(1)	4.4(2)	1.4(1)	1.3(1)	Quadrupole
$\frac{25}{2}^- \rightarrow \frac{21}{2}^-$	985.0(1)	1.7(1)	1.2(2)	1.1(2)	Quadrupole
$\frac{29}{2}^- \rightarrow \frac{25}{2}^-$	1047.5(1)	1.04(8)	1.3(7)	1.1(7)	Quadrupole
$\frac{13}{2}^- \rightarrow \frac{13}{2}^+$	817.3(1)	2.1(1)	1.3(0.2)	1.0(2)	$\Delta I = 0$ dipole
Band "neg1"					
$\frac{21}{2}^{(-)} \rightarrow \frac{19}{2}^+$	820.1(1)	6.7(4)	0.60(4)	0.85(6)	Dipole
$\frac{23}{2}^{(-)} \rightarrow \frac{21}{2}^{(-)}$	695.4(1)	6.3(3)	0.76(6)	0.81(7)	Dipole
$\frac{25}{2}^{(-)} \rightarrow \frac{23}{2}^{(-)}$	277.9(1)	31(2)	0.69(3)	0.99(3)	Dipole
$\frac{27}{2}^{(-)} \rightarrow \frac{25}{2}^{(-)}$	338.0(1)	23(1)	0.65(2)	0.93(3)	Dipole[a]
$\frac{29}{2}^{(-)} \rightarrow \frac{27}{2}^{(-)}$	530.7(1)	18.8(9)	0.61(3)	0.81(4)	Dipole
$\frac{29}{2}^{(-)} \rightarrow \frac{25}{2}^{(-)}$	868.7(1)	9.01(5)	1.21(7)	1.11(7)	Quadrupole[b]
$\frac{31}{2}^{(-)} \rightarrow \frac{27}{2}^{(-)}$	867.9(1)	4.1(1)	1.21(7)	1.11(7)	Quadrupole
$\frac{31}{2}^{(-)} \rightarrow \frac{29}{2}^{(-)}$	337.2(1)	14.5(8)	0.65(2)	0.93(3)	Dipole
$\frac{33}{2}^{(-)} \rightarrow \frac{31}{2}^{(-)}$	590.3(1)	18.8(9)	0.71(3)	0.93(4)	Dipole
$\frac{33}{2}^{(-)} \rightarrow \frac{29}{2}^{(-)}$	927.7(1)	12.7(7)	1.34(8)	1.19(8)	Quadrupole
$\frac{37}{2}^{(-)} \rightarrow \frac{33}{2}^{(-)}$	1341.2(1)	24(1)	1.15(6)	1.09(6)	Quadrupole
$\frac{41}{2}^{(-)} \rightarrow \frac{37}{2}^{(-)}$	892.1(1)	21(1)	1.37(6)	1.23(5)	Quadrupole
$\frac{23}{2}^{(-)} \rightarrow \frac{21}{2}^+$	1117.3(1)	36(2)	0.66(2)	0.90(3)	Dipole
Band "neg2"					
$\frac{43}{2}^{(-)} \rightarrow \frac{41}{2}^{(-)}$	849.9(1)	7.7(4)	0.64(7)	1.0(0.1)	Dipole
$\frac{47}{2}^{(-)} \rightarrow \frac{43}{2}^{(-)}$	1305.3(1)	4.5(2)	1.3(2)	1.2(2)	Quadrupole
$\frac{51}{2}^{(-)} \rightarrow \frac{47}{2}^{(-)}$	1447.3(1)	2.1(1)	1.3(4)	1.2(3)	Quadrupole
Band "pos1"					
$\frac{33}{2}^+ \rightarrow \frac{29}{2}^+$	1052.7(1)	3.1(3)	1.4(1)	1.1(1)	Quadrupole[c]
$\frac{37}{2}^+ \rightarrow \frac{33}{2}^+$	1205.3(1)	3.1(2)	1.2(1)	1.0(1)	Quadrupole[d]
Band "pos2"					
$\frac{13}{2}^+ \rightarrow \frac{9}{2}^+$	778.1(1)	100(7)			
$\frac{17}{2}^+ \rightarrow \frac{13}{2}^+$	860.0(1)	91(5)	1.35(4)	1.21(4)	Quadrupole
$\frac{21}{2}^+ \rightarrow \frac{17}{2}^+$	891.5(1)	47(2)	1.21(4)	1.20(4)	Quadrupole
$\frac{25}{2}^+ \rightarrow \frac{21}{2}^+$	993.4(1)	13.4(7)	1.15(6)	1.07(6)	Quadrupole
$\frac{29}{2}^+ \rightarrow \frac{25}{2}^+$	1041.2(1)	10.5(6)	1.14(8)	1.03(8)	Quadrupole
$\frac{33}{2}^+ \rightarrow \frac{29}{2}^+$	1073.5(1)	6.2(0.4)	1.4(3)	1.2(3)	Quadrupole
$\frac{37}{2}^+ \rightarrow \frac{33}{2}^+$	1128.0(1)	4.0(2)	1.3(3)	1.1(3)	Quadrupole
$\frac{19}{2}^+ \rightarrow \frac{17}{2}^+$	493.3(1)	46(2)	0.71(2)	0.92(3)	Dipole
$\frac{21}{2}^+ \rightarrow \frac{19}{2}^+$	398.1(1)	20(1)	0.81(3)	0.96(4)	Dipole
$\frac{23}{2}^+ \rightarrow \frac{21}{2}^+$	556.4(1)	11(1)	0.73(7)	0.92(8)	Dipole
$\frac{25}{2}^+ \rightarrow \frac{23}{2}^+$	436.7(1)	5.8(3)	0.65(4)	0.76(4)	Dipole

TABLE I. (*Continued*.)

$I_i \rightarrow I_f$	E_γ (keV)	I_γ	ADO (32°/90°)	ADO (58°/90°)	Multipolarity
$\frac{29}{2}^+ \rightarrow \frac{27}{2}^+$	363.6(1)	3.4(2)	0.54(5)	0.73(7)	Dipole
$\frac{33}{2}^+ \rightarrow \frac{31}{2}^+$	381.1(1)	2.4(1)	0.55(6)	0.77(8)	Dipole
$\frac{23}{2}^+ \rightarrow \frac{19}{2}^+$	954.8(1)	19(1)	1.37(7)	1.23(6)	Quadrupole
$\frac{27}{2}^+ \rightarrow \frac{23}{2}^+$	1114.3(1)	12.6(7)	1.39(8)	1.20(7)	Quadrupole
$\frac{31}{2}^+ \rightarrow \frac{27}{2}^+$	1055.8(1)	5.8(3)	1.3(2)	1.3(2)	Quadrupole
Band "pos3"					
$\frac{27}{2}^+ \rightarrow \frac{23}{2}^+$	1251.4(1)	3.5(2)	1.3(2)	1.2(3)	Quadrupole
$\frac{31}{2}^+ \rightarrow \frac{27}{2}^+$	1052.9(1)	3.3(2)	1.4(0.1)	1.1(1)	Quadrupole
$\frac{35}{2}^+ \rightarrow \frac{31}{2}^+$	1205.2(1)	2.3(1)	1.2(1)	1.0(1)	Quadrupole
$\frac{39}{2}^+ \rightarrow \frac{35}{2}^+$	1148.0(1)	1.8(1)	1.1(2)	1.1(0.2)	Quadrupole

[a]Mixed with a 337.2-keV transition.
[b]Mixed with a 867.9-keV transition.
[c]Mixed with a 1052.9-keV transition.
[d]Mixed with a 1205.2-keV transition.

Sec. III concerns the interpretation of the observed $\frac{51}{2}^{(-)}$ state as a terminating state and the property of the band based on the $p_{1/2}$ proton orbital from the two different viewpoints, one of which is a weakly deformed soft rotor with spin alignments and the other is vibrational-to-rotational evolution along the band. Lastly, a summary is given in Sec. IV.

II. EXPERIMENTAL METHODS AND RESULTS

In-beam γ-ray spectroscopy was performed on ^{99}Rh through the reaction ^{68}Zn(^{37}Cl, $\alpha 2n$). The data on ^{99}Rh was obtained as a by-product of the experiment which was originally intended for the study of ^{101}Pd [11]. An enriched ^{68}Zn foil with a thickness of 9 mg/cm^2 was bombarded with a 125-MeV ^{37}Cl beam provided by the tandem accelerator at the Japan Atomic Energy Agency (JAEA), whereby γ rays emitted from the excited states were detected with an array of 12 HPGe detectors with bismuth germanate Compton suppressors (GEMINI) [12]. The HPGe detectors were placed at angles of 32°, 58°, 90°, 122°, and 148° with respect to the beam direction. The energy resolution of the HPGe detectors was 1.8–2.7 keV at 1.3 MeV, and the experimental data were recorded on magnetic tapes on an event-by-event basis when two or more detectors were fired. A total of 2.9×10^8 events were collected during 3 days of beam time. Multiple γ-γ coincidence events were sorted into E_γ-E_γ matrices, and the level scheme was constructed from these matrices using software written by Radford [13]. The relative intensities of γ rays were obtained from the gated spectra. For the level spin assignments, we used the γ-ray coincidence intensity ratios $I(\gamma_1$:32° or 148°, γ_2:all)/$I(\gamma_1$:90°, γ_2:all), and $I(\gamma_1$:58° or 122°, γ_2:all)/$I(\gamma_1$:90°, γ_2:all) [angular distribution from oriented nuclei (ADO) ratios] [14]. Here, $I(\gamma_1$:θ, γ_2:all) corresponds to the γ-ray coincidence intensity observed by the detectors at an angle θ by setting gates on the detectors to allow for any angle. To obtain these ratios, we sorted γ-γ coincidence events to three asymmetric matrices whose x axes were the γ-ray energies in the detector at 32° or 148°, 58° or 122°, and 90°, while the y axes for these matrices were the γ-ray energies in the detector at any position. Although several transitions exhibit multiplet structures, ADO ratios were obtained separately for individual components whenever it was possible to set the proper gate. Typical ADO(32°/90°) ratios observed for the known γ rays in this experiment were 1.3 for stretched quadrupole transitions and 0.7 for stretched pure dipole transitions. Therefore, we assigned the stretched quadrupole transition (stretched dipole transition) to ratios around 1.3 (around 0.7) for the new γ rays.

The total projection spectrum of the E_γ-E_γ matrix, which is shown in Fig. 1, indicates that although ^{101}Pd was a main product, ^{99}Rh was also produced appreciably in the present reaction.

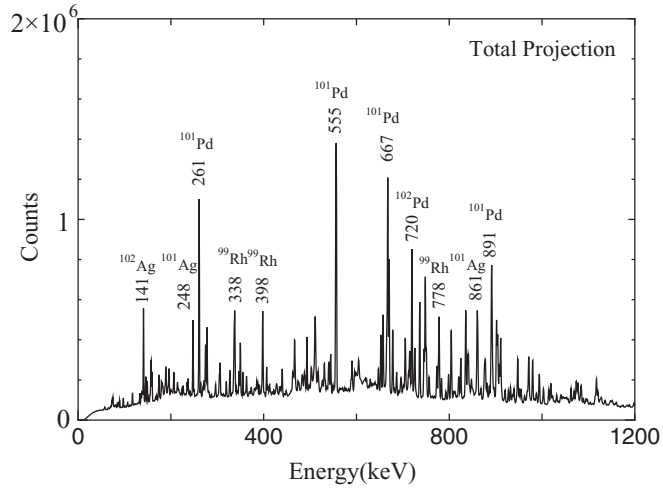

FIG. 1. Total projection spectrum of the E_γ-E_γ matrix. Only prominent transitions of main reaction products are marked with their energies and nuclide symbols.

There were two experimental studies on high-spin states of ^{99}Rh previous to this experiment. One was through the reaction ^{89}Y(^{16}O, $\alpha 2n$) [8] and the other was through the reaction ^{66}Zn(^{37}Cl, $2p2n$) [9]. Four bands were found in total in the former experiment. The two bands, each based on $\pi p_{1/2}$ and $\pi g_{9/2}$, were observed up to $\frac{21}{2}^-$ and $\frac{25}{2}^+$, respectively. The two side bands, one with positive parity and the other with no parity assignment, were observed from $\frac{19}{2}^+$ to $\frac{31}{2}^+$ and from $\frac{23}{2}$ to $\frac{37}{2}$, respectively. In the latter experiment, while the four bands mentioned above were also observed, the highest spin value of the side band with no parity assignment was modified to $\frac{41}{2}$ and the band based on $\pi g_{9/2}$ was claimed to be extended to $\frac{49}{2}^+$. However, there was an incomprehensible point concerning the level scheme proposed in Ref. [9]. That is, while the higher-spin part of the band based on $\pi g_{9/2}$ which was only weakly populated was extended to $\frac{49}{2}^+$, a rather strongly populated side band with no parity assignment which began at $\frac{23}{2}$ ceased to exist at $\frac{41}{2}$ abruptly. Therefore, in the present study, E_γ-E_γ matrix was analyzed carefully on the coincidence relations including the yrast and side bands mentioned above.

The properties of the γ rays observed in this experiment are summarized in Table I, and the level scheme for ^{99}Rh established in this experiment is shown in Fig. 2, where the observed bands are labeled "$p_{1/2}$", "neg1", "neg2", "pos1", "pos2", and "pos3" from left to right. Examples of γ-γ coincidence spectra are presented in Figs. 3–6 as an illustration of the band structure in the proposed level scheme.

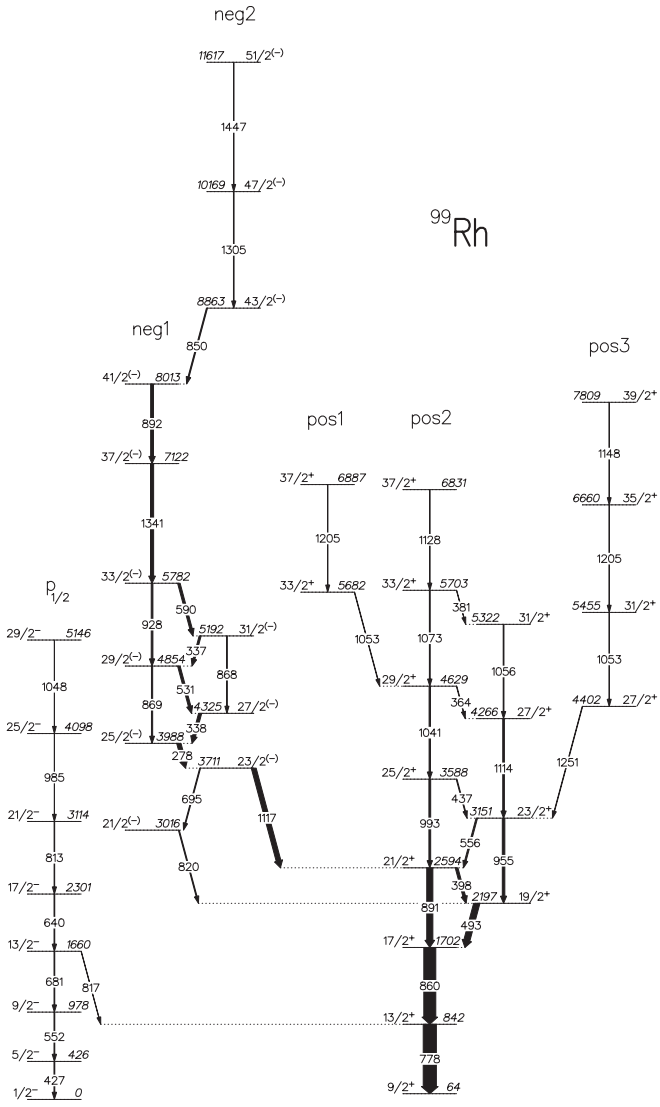

FIG. 2. Level scheme of ^{99}Rh proposed based on analysis of the E_γ-E_γ matrix. The bands are labeled "$p_{1/2}$", "neg1", "neg2", "pos1", "pos2", and "pos3" from left to right for reference in the text.

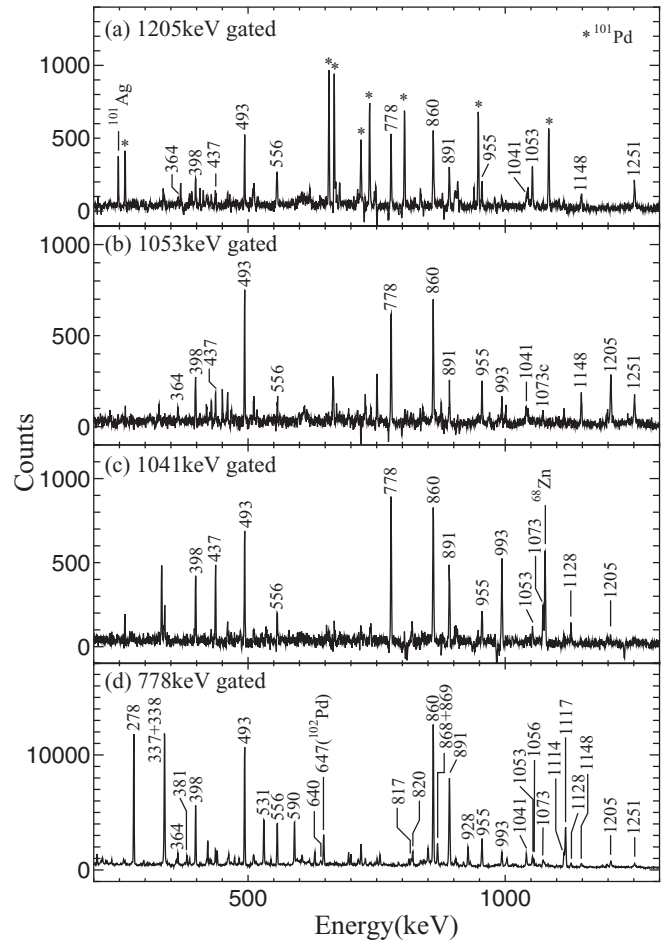

FIG. 3. Examples of γ-γ coincidence spectra obtained by setting gates on the transitions within the positive-parity bands. These spectra were obtained from the E_γ-E_γ matrix and provide support for the branching at the upper part of the positive-parity bands. Energy values are given above the peaks in units of keV. (a) A spectrum obtained by setting a gate on the 1205-keV transition from $\frac{37}{2}^+$ to $\frac{33}{2}^+$ in band "pos1", which includes the one from $\frac{35}{2}^+$ to $\frac{31}{2}^+$ in band "pos3". (b) A spectrum obtained by setting a gate on the 1053-keV transition from $\frac{33}{2}^+$ to $\frac{29}{2}^+$ in band "pos1", which includes the one from $\frac{31}{2}^+$ to $\frac{27}{2}^+$ in band "pos3". The peak labeled "1073c" is due to a contamination in the gate. (c) A spectrum obtained by setting a gate on the 1041-keV transition from $\frac{29}{2}^+$ to $\frac{25}{2}^+$ in band "pos2". The peak with the symbol "^{68}Zn" is due to the Coulomb excitation of the target. (d) A spectrum obtained by setting a gate on the 778-keV transition from $\frac{13}{2}^+$ to $\frac{9}{2}^+$ in band "pos2".

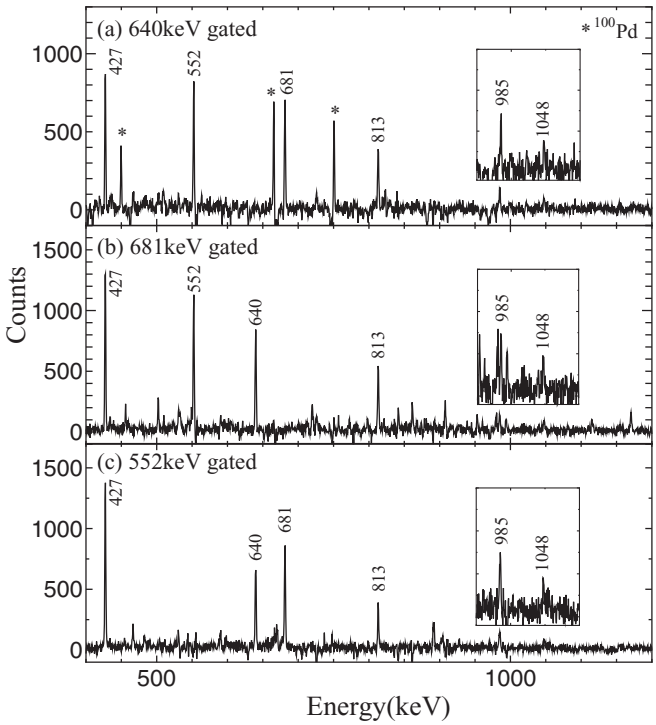

FIG. 4. Examples of γ-γ coincidence spectra obtained by setting gates on the transitions within band "$p_{1/2}$". These spectra can be used to extend the band to higher-spin states. Energy values are given above the peaks in units of keV. Each inset shows a vertically expanded spectrum for the high-energy region around 1000 keV. (a) A spectrum obtained by setting a gate on the 640-keV transition from $\frac{17}{2}^-$ to $\frac{13}{2}^-$ in band "$p_{1/2}$". (b) A spectrum obtained by setting a gate on the 681-keV transition from $\frac{13}{2}^-$ to $\frac{9}{2}^-$ in band "$p_{1/2}$". (c) A spectrum obtained by setting a gate on the 552-keV transition from $\frac{9}{2}^-$ to $\frac{5}{2}^-$ in band "$p_{1/2}$".

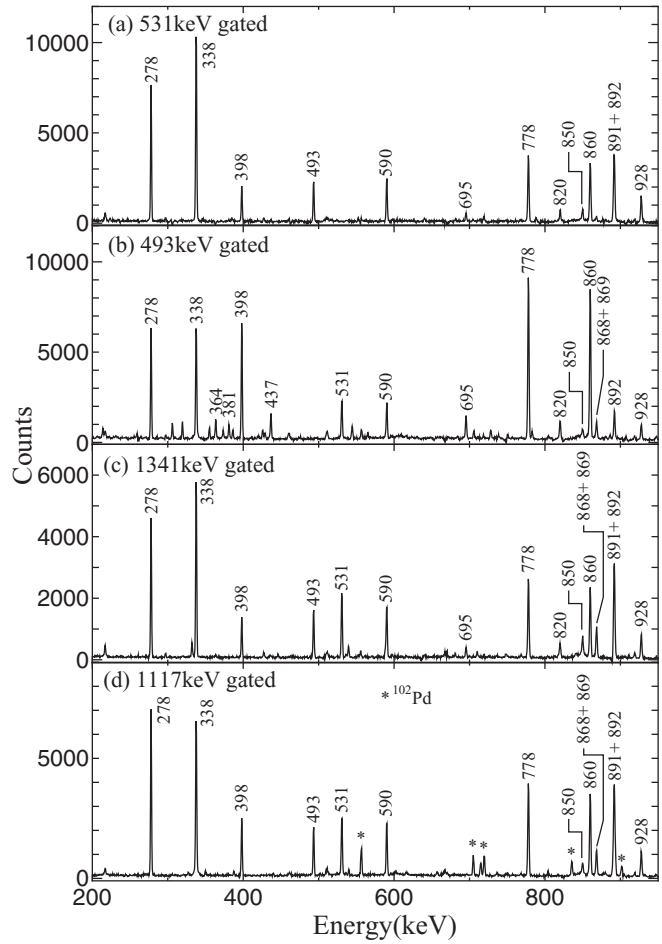

FIG. 5. Lower energy parts of γ-γ coincidence spectra obtained by setting gates on the transitions within the proposed negative-parity band. These spectra can be used to extend the band to higher-spin states. Energy values are given above the peaks in units of keV. (a) A spectrum obtained by setting a gate on the 531-keV transition from $\frac{29}{2}^{(-)}$ to $\frac{27}{2}^{(-)}$ in band "neg1". (b) A spectrum obtained by setting a gate on the 493-keV transition from $\frac{19}{2}^+$ to $\frac{17}{2}^+$ in band "pos2". (c) A spectrum obtained by setting a gate on the 1341-keV transition from $\frac{37}{2}^{(-)}$ to $\frac{33}{2}^{(-)}$ in band "neg1". (d) A spectrum obtained by setting a gate on the 1117-keV transition from $\frac{23}{2}^{(-)}$ to $\frac{21}{2}^+$ between bands "neg1" and "pos2".

First, the coincidence relations are described relating to the positive-parity bands on the basis of spectra in Fig. 3. A spectrum obtained by setting a gate on the 1205-keV transition from $\frac{37}{2}^+$ to $\frac{33}{2}^+$, or from $\frac{35}{2}^+$ to $\frac{31}{2}^+$, is shown in Fig. 3(a), which suggests that the 1053-, 1148-, and 1251-keV transitions are in cascade and the 1073- and 1128-keV transitions are in parallel with the 1205-keV transition. Furthermore, the spectrum obtained by setting a gate on the 1053-keV transition from $\frac{31}{2}^+$ to $\frac{27}{2}^+$[see Fig. 3(b)] confirms the cascade relation between the 1053- and 1148-keV or 1251-keV transitions. Consequently, the present data suggest the cascade of the 1052-, 1205-, 1073-, and 1128-keV transitions claimed in [9] should be replaced with the two parallel cascades of 1053, 1205 keV and 1073, 1128 keV. A 1197-keV transition placed at the top of the $\pi g_{9/2}$ band in [9] has not been identified in the present data. Moreover, the spectrum in Fig. 3(c), obtained by setting a gate on the 1041-keV transition from $\frac{29}{2}^+$ to $\frac{25}{2}^+$, clearly suggests that the 1148- and 1251-keV transitions are in parallel with the gate. To fulfill the coincidence relations mentioned above, two cascades of 1205- and 1053-keV transitions turn out to be necessary, one of which is in cascade and the other is in parallel with the 1041-keV transition. Finally, it is clear that the spectrum in Fig. 3(d), obtained by setting a gate on the 778-keV transition from $\frac{13}{2}^+$ to $\frac{9}{2}^+$, is consistent with the other three spectra considering the fact that the gate is the lowest transition in the band.

Then the coincidence relations are described next relating to band "$p_{1/2}$" on the basis of spectra in Fig. 4. Spectra obtained by setting gates on the 640-keV transition from $\frac{17}{2}^-$ to $\frac{13}{2}^-$, the 681-keV transition from $\frac{13}{2}^-$ to $\frac{9}{2}^-$, and the 552-keV transition from $\frac{9}{2}^-$ to $\frac{5}{2}^-$ are shown in Figs. 4(a), 4(b), and 4(c), respectively. These spectra suggest that the 985- and 1048-keV transitions are in cascade with the gates.

Lastly the coincidence relations are described relating to bands "neg1" and "neg2" on the basis of spectra in Figs. 5 (lower energy parts) and 6 (higher energy parts). Spectra obtained by setting gates on the 531-keV transition from

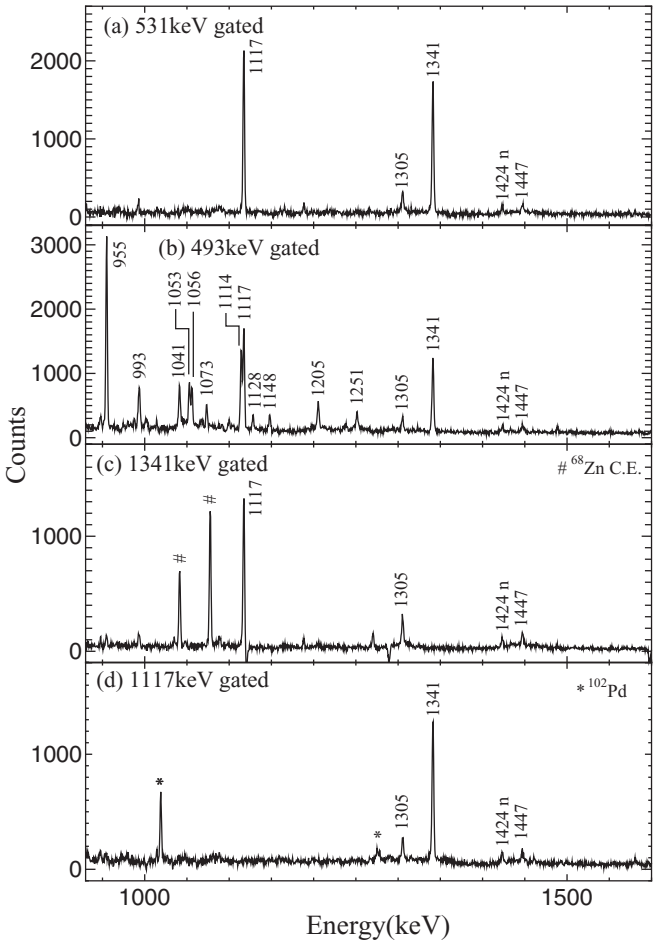

FIG. 6. Higher energy parts of the same γ-γ coincidence spectra as those in Fig. 5. C.E. stands for Coulomb excitation. A peak marked 1424n is the transition of 1424 keV which could not be placed in the level scheme while appearing commonly in the spectra.

$\frac{29}{2}^{(-)}$ to $\frac{27}{2}^{(-)}$, the 493-keV from $\frac{19}{2}^{+}$ to $\frac{17}{2}^{+}$, the 1341-keV from $\frac{37}{2}^{(-)}$ to $\frac{33}{2}^{(-)}$, and the 1117-keV from $\frac{23}{2}^{(-)}$ to $\frac{21}{2}^{+}$ are shown in Figs. 5(a), 5(b), 5(c), and 5(d), respectively. It can be seen that the 892-, 850-, 1305-, and 1447-keV transitions appear commonly in all of these spectra. The other transitions within bands "neg1" and "neg2" are also seen in these spectra. Especially, the 892-keV transition from $\frac{41}{2}^{(-)}$ to $\frac{37}{2}^{(-)}$ is separated from the 891-keV transition from $\frac{21}{2}^{+}$ to $\frac{17}{2}^{+}$ in the spectrum in Fig. 5(b) (493-keV gated), and the 868-keV transition from $\frac{31}{2}^{(-)}$ to $\frac{27}{2}^{(-)}$ and the 869-keV transition from $\frac{29}{2}^{(-)}$ to $\frac{25}{2}^{(-)}$ disappear in the spectrum in Fig. 5(a) (531-keV gated). Although the peak marked 1424n appears commonly in all of the spectra in Fig. 6, this transition could not be placed with certainty in the level scheme since the transitions of similar energy exist in ^{101,102}Pd.

Parity assignment could not be made for the side band beginning at $\frac{23}{2}$ in either of the previous studies mentioned earlier [8,9] without either γ-ray linear polarization or conversion electron measurements. Although the same is true in the present experiment, negative parity has been assigned tentatively for that band based on the following arguments.

(i) The 1117-keV transition between the side and yrast bands has a pure dipole character.
(ii) There is a similar transition between 9^- of the side band and 8^+ of the yrast band in ^{98}Ru [4] which is even core for ^{99}Rh. Taking a weak-coupling view, the $\frac{23}{2}^-$ and $\frac{21}{2}^+$ states in ^{99}Rh can be made by coupling $\pi(g_{9/2})_{m=5/2}$ to the even core.
(iii) There exists a similar negative-parity side band decaying to the $\frac{21}{2}^+$ state of the yrast band through a strong $E1$ transition of 750 keV in ^{101}Rh [5].

Parity assignments for the other bands turned out to be consistent with the observed ADO ratios of γ transitions.

Bands "$p_{1/2}$", "neg1", and "pos2" were known from the previous studies [8,9] to $\frac{21}{2}^-$, $\frac{41}{2}$ with no parity assignment, and $\frac{29}{2}^+$, respectively. In the present experiment, we extended band "$p_{1/2}$" to higher spins by $4\hbar$. Band "neg2" is a new band which was found to decay to band "neg1". Although band "neg1" was already observed in the previous studies, it

TABLE II. $B(M1)/B(E2)$ ratios for transitions in bands "pos2" and "neg1". Dipole and quadrupole transitions are assumed to be pure $M1$ and pure $E2$ transitions, respectively. Values for corresponding transitions in ^{101}Rh are also listed for comparison. Data on ^{101}Rh are taken from Ref. [10].

	Initial spin I_i	$\frac{B(M1)}{B(E2)}(\frac{\mu_N}{eb})^2$
^{99}Rh		
	Band"pos2"	
	$\frac{21}{2}^+$	2.7(2)
	$\frac{23}{2}^+$	1.8(2)
	$\frac{25}{2}^+$	3.5(3)
	$\frac{29}{2}^+$	5.8(4)
	$\frac{33}{2}^+$	7.1(6)
	Band "neg1"	
	$\frac{29}{2}^{(-)}$	4.8(3)
	$\frac{33}{2}^{(-)}$	3.4(3)
^{101}Rh		
	$\frac{13}{2}^+$	8.9(6)
	$\frac{15}{2}^+$	1.3(1)
	$\frac{17}{2}^+$	7.2(5)
	$\frac{21}{2}^+$	1.6(1)
	$\frac{27}{2}^-$	7.8(6)
	$\frac{29}{2}^-$	4.6(3)
	$\frac{31}{2}^-$	8.9(6)
	$\frac{33}{2}^-$	6.4(5)
	$\frac{35}{2}^-$	2.6(2)
	$\frac{37}{2}^-$	5.8(4)
	$\frac{41}{2}^-$	9.8(8)

TABLE III. Lowest terminating configurations with negative parity observed so far in neighboring nuclei and the corresponding possible one in ^{99}Rh. For the meaning of shorthand notation for possible configurations, see text.

Nuclide	Configuration (shorthand) $[p, n]$	Terminating spin	Configuration (full)
^{98}Ru	[4, 1]	25^-	$\pi(g_{9/2})^4_{12}\nu(d_{5/2}g_{7/2})^3_{15/2}(h_{11/2})^1_{11/2}$
^{99}Rh	[5, 1]	$\frac{51}{2}^-$	$\pi(g_{9/2})^5_{25/2}\nu(d_{5/2}g_{7/2})^3_{15/2}(h_{11/2})^1_{11/2}$
^{99}Ru	[4, 1]	$\frac{55}{2}^-$	$\pi(g_{9/2})^4_{12}\nu(d_{5/2}g_{7/2})^4_{10}(h_{11/2})^1_{11/2}$
^{100}Ru	[4, 1]	28^-	$\pi(g_{9/2})^4_{12}\nu(d_{5/2}g_{7/2})^5_{21/2}(h_{11/2})^1_{11/2}$
^{101}Rh	[5, 1]	$\frac{57}{2}^-$	$\pi(g_{9/2})^5_{25/2}\nu(d_{5/2}g_{7/2})^5_{21/2}(h_{11/2})^1_{11/2}$

was assigned negative parity in this experiment based on the arguments described earlier. The lower part of band "pos2" was already known in the previous studies as well. Bands "pos1" and "pos3" and the higher part of band "pos2" are those constructed by rearranging the transitions which were placed on top of the lower part of band "pos2" in Ref. [9].

Several $M1$ transitions have been observed within bands "neg1" and "pos2". The properties of those transitions are summarized in terms of $B(M1)/B(E2)$ ratios in Table II. Values for corresponding transitions in ^{101}Rh are also listed for comparison. The fact that the decaying transitions from the corresponding states in ^{99}Rh and ^{101}Rh have similar $B(M1)/B(E2)$ ratios seems to support the parity assignment in the present study.

III. DISCUSSION

Since the main new results in the present study are the observation of band "neg2" and the extension of band "$p_{1/2}$", discussions will be given on these bands first. The rearrangement of the upper part of the positive-parity bands to "pos1", "pos2", and "pos3" is also an important finding in the present study. A discussion on the positive-parity bands is presented next.

A. Interpretation of band "neg2" as a possible terminating configuration

As described in Sec. I, band termination has been analyzed theoretically mainly based on the configuration-dependent cranked Nilsson-Strutinsky approach [1]. Since relevant high-j orbitals in the $A \sim 100$ region are $\pi g_{9/2}$ and $\nu h_{11/2}$, the shorthand notation $[p, n]$ is usually used for assigning possible terminating configurations. The lowest terminating configurations with negative parity observed so far in the neighboring Ru and Rh isotopes are listed in Table III [4,5]. These terminating states were populated through the similar reactions at similar energies to the present experiment. Therefore, if the corresponding one is not observed in ^{99}Rh, that fact needs a theoretical explanation. Since the slope of excitation energy versus spin curve in a rotating frame is helpful to characterize a terminating configuration qualitatively, the excitation energy relative to a rigid rotor reference is shown as a function of the spin for the negative-parity bands of ^{99}Rh in Fig. 7(a) and compared with the corresponding curves for the lowest terminating bands of ^{98,99,100}Ru [4] and ^{101}Rh [5] in Fig. 7(b). It is clear that there is a close similarity between the slope for band "neg2" in ^{99}Rh and those at high spin for the corresponding bands in ^{98,99,100}Ru and ^{101}Rh. More specifically, the excitation energies observed for the terminating configuration [5, 1] in ^{99,101}Rh are compared with those for [4, 1] in ^{98,100}Ru in Table IV [4,5]. Here, the excitation energy of the configuration [5, 1] is shown with respect to that of the $\frac{9}{2}^+$ state. The configuration [5, 1] is different from [4, 1] only by an additional $\pi g_{9/2}$. If the band "neg2" corresponds to the configuration [5, 1], its excitation energy should be similar to that of [4, 1] in ^{98}Ru except for the interaction energy involving the additional $\pi g_{9/2}$. This

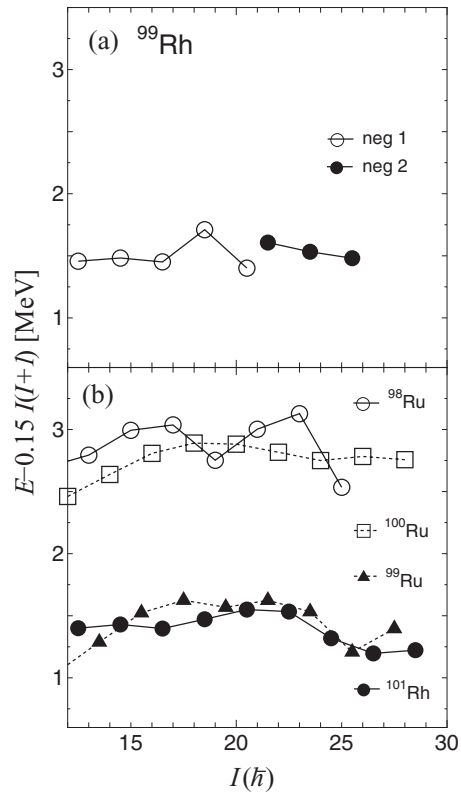

FIG. 7. Excitation energy relative to a rigid rotor reference as a function of the spin for (a) the negative-parity bands in ^{99}Rh and (b) the lowest terminating bands whose configurations are listed in Table III in neighboring nuclei (^{98,99,100}Ru [4] and ^{101}Rh [5]).

TABLE IV. Comparison of the excitation energies observed for the terminating configurations [4, 1] (^{98,100}Ru) and [5, 1] (^{99,101}Rh). The excitation energy of the $\frac{9}{2}^+$ state is subtracted from that of the configuration [5, 1]. Δ is a difference of excitation energies between the configurations [4, 1] and [5, 1].

Configuration	[4, 1]		[5, 1]		
Nuclide	^{98}Ru		^{99}Rh		
	I^π	E_x (keV)	I^π	E_x (keV)	Δ (keV)
	25^-	12285	$\frac{51}{2}^{(-)}$	11553	732
	23^-	11408	$\frac{47}{2}^{(-)}$	10105	1303
	21^-	9933	$\frac{43}{2}^{(-)}$	8799	1134
Nuclide	^{100}Ru		^{101}Rh		
	I^π	E_x (keV)	I^π	E_x (keV)	Δ (keV)
	28^-	14936	$\frac{57}{2}^-$	13679	1257
	26^-	13312	$\frac{53}{2}^-$	11973	1339
	24^-	11749	$\frac{49}{2}^-$	10535	1214

interaction energy might be reasonably estimated from the difference of excitation energies between the configuration [5, 1] in ^{101}Rh and the configuration [4, 1] in ^{100}Ru which is listed as Δ in the rightmost column in Table IV. It is clear that the Δ values for ^{98}Ru and ^{99}Rh are quite similar to those for ^{100}Ru and ^{101}Rh, except for the highest spin state. This irregularity at the highest spin state seems to reflect the abrupt lowering of the 25^- state in ^{98}Ru which can be seen in Fig. 7(b). Consequently, it is possible to interpret the $\frac{51}{2}^{(-)}$ state in band "neg2" as the terminating state for the configuration [5, 1] in ^{99}Rh.

B. Two possible scenarios for the structural change in the "$p_{1/2}$" band: Weakly deformed soft rotor with spin alignments vs vibrational-to-rotational evolution

Since the $\pi p_{1/2}$ band has been extended to higher spin by 4 $\hbar$ in the present study, it is appropriate to address the structural evolution along the band. There are two possible scenarios, one of which is a weakly deformed soft rotor with spin alignments and the other is a vibrational to rotational evolution.

To illuminate the alignment properties, aligned angular momenta (i_x) are plotted as functions of rotational frequency for the $\pi p_{1/2}$ bands in ^{99,101,103}Rh in Fig. 8. There is an alignment gain of about 3 $\hbar$ around $\hbar\omega = 0.35$ MeV in ^{99}Rh which can be attributed to the first $\pi g_{9/2}$ crossing based on the cranked shell model calculations [9]. It is reasonably seen that this crossing is delayed due to a slightly larger deformation in ^{101,103}Rh. An upbend around $\hbar\omega = 0.50$ MeV in ^{99}Rh can be interpreted to be associated with the alignment of a $g_{7/2}$ neutron pair in this line of reasoning.

However, there is another possible scenario for the structural change invoking no structural preconceptions such as a permanently deformed rotor. Regan *et al.* [20] suggested a simple ratio of $E_\gamma(I \to I-2)$ to spin I (called R hereafter) might be a good indicator to highlight the evolution from vibrational to rotational structure along the yrast line in

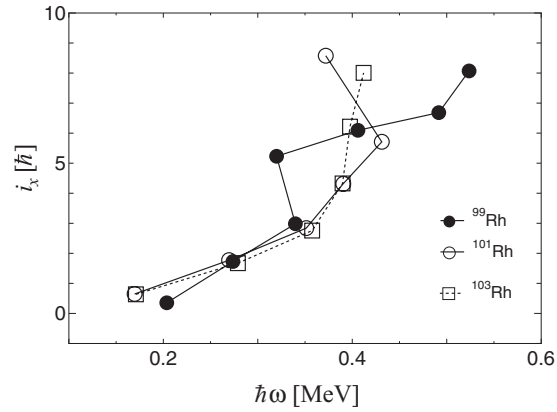

FIG. 8. Comparison of aligned angular momenta (i_x) for the $\pi p_{1/2}$ bands in ^{99,101,103}Rh [10,15,16]. A Harris reference with $J_0 = 7.0\hbar^2$ MeV^{-1} and $J_1 = 15.7\hbar^4$ MeV^{-3} has been used.

transitional nuclei. For example, R is given as $\frac{\hbar\omega}{I}$ for a perfect harmonic vibrator, while $\frac{\hbar^2}{2J}(4 - \frac{2}{I})$ for an axially symmetric rotor, where $\hbar\omega$ is the phonon energy and J is the moment of inertia. Therefore vibrational and rotational characters can be discriminated by the sign of curvature for the R-I curve. This approach, called the E-GOS (E-gamma over spin) curve, was applied to the yrast cascades in the $A \sim 110$ region and a clear transition from vibrational to rotational motion was found [20]. Since ^{99}Rh is around the lower edge of the $A \sim 110$ region, the E-GOS curve seems useful to clarify the structural evolution in the $\pi p_{1/2}$ band. Here R is calculated as $\frac{E_\gamma}{I-I_0}$ to apply to odd-mass nuclei, where I_0 stands for the spin value of the bandhead. Figure 9(a) shows the E-GOS curves for the $\pi p_{1/2}$ bands in ^{95,97,99}Tc [17–19], and Fig. 9(b) for those in ^{99,101,103}Rh [10,15,16]. It is clearly seen that the sign of curvature has changed around 8 $\hbar$ in ^{95,97}Tc and ^{99}Rh, which are nuclei with $N = 54$ or less. This vibrational-to-rotational transition can be explained by the population of the 8^+ state with maximally aligned two $g_{9/2}$ proton orbitals. The more spherical nucleus can be more easily polarized and a weakly deformed shape can be stabilized by such alignments.

Therefore the two scenarios are conceivable for the structural change in the "$p_{1/2}$" band. However, it is the alignment

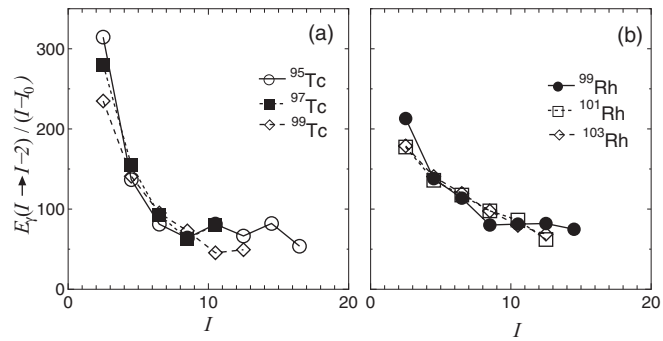

FIG. 9. E-GOS curves for the $\pi p_{1/2}$ bands in (a) ^{95,97,99}Tc [17–19] and (b) ^{99,101,103}Rh [10,15,16]. Here I_0 stands for the spin value of the bandhead.

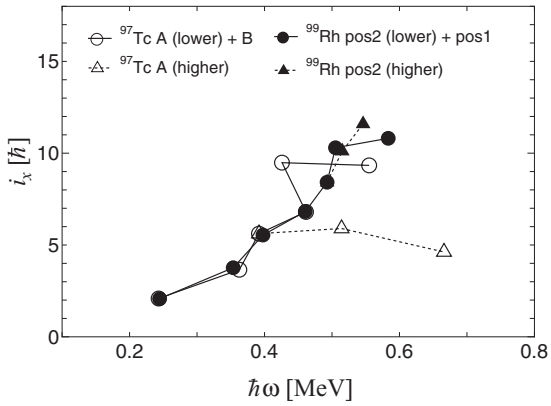

FIG. 10. Comparison of aligned angular momenta (i_x) for the positive-parity bands in ^{99}Rh and ^{97}Tc. A Harris reference with $J_0 = 6.0\hbar^2$ MeV^{-1} and $J_1 = 15.7\hbar^4$ MeV^{-3} has been used. The data and the band labels for ^{97}Tc are taken from Ref. [21].

of two $g_{9/2}$ protons that causes this structural change in either case.

C. Properties of the positive-parity bands

Since the higher-spin part of the $\pi g_{9/2}$ band, which was claimed to extend to $\frac{49}{2}^+$ in Ref. [9], has been replaced with the two parallel cascades of 1053, 1205 keV and 1073, 1128 keV in the present study, an analysis in terms of cranked shell model taken up there should be reexamined. Figure 10 illustrates the alignments (i_x) for bands "pos1" and "pos2" as functions of rotational frequency ($\hbar\omega$). Similar parallel cascades are known in ^{97}Tc [21] which is the odd-Z isotone of ^{99}Rh. Therefore, the alignments for those bands in ^{97}Tc are also shown for comparison. It is seen that there is an alignment gain of about 3.5 $\hbar$, around $\hbar\omega = 0.43$ MeV in ^{97}Tc, and 0.50 MeV in ^{99}Rh. Since the first proton crossing is blocked, this upbend is attributed to the alignment of a $g_{7/2}$ neutron pair in Refs. [9,21] based on the cranked shell model calculations. This observation is consistent with the upbend around $\hbar\omega = 0.50$ MeV observed in the "$p_{1/2}$" band in Fig. 8. The backbend, which was claimed to be observed at about $\hbar\omega = 0.57$ MeV and interpreted as due to the second $\pi g_{9/2}$ crossing in Ref. [9], has not been observed in the present experiment. It is worth while mentioning that the difference between the curves for the two bands in ^{97}Tc is almost removed by adding two protons in ^{99}Rh.

The band "pos3" seems $\alpha = -\frac{1}{2}$ partner of the band "pos1" taking account of its spin and excitation energy. However, since linking transitions have not been observed between signature partners, it is difficult to judge whether these are signature partners from the present data.

IV. SUMMARY

We presented the results of a study on the high-spin states of ^{99}Rh, which were obtained through in-beam γ-ray spectroscopy using the reaction ^{68}Zn(^{37}Cl,$\alpha 2n$). Negative parity has been tentatively assigned to the known band decaying through a pure dipole transition to the $\pi g_{9/2}$ band, based on the structural similarities within neighboring nuclei. A new band has been found to decay to the negative-parity band mentioned above and is interpreted as a possible terminating configuration. The band based on the $\pi p_{1/2}$ orbital has been extended to higher-spin state, the structure of which is discussed from the different viewpoints such as a weakly deformed soft rotor with spin alignments and a vibrational-to-rotational evolution along the band. The band based on the $\pi g_{9/2}$ orbital, which was already known from the previous studies, has been reorganized into three parallel cascades in the higher-spin part. The structure of this band is reanalyzed based on the alignment plot using the revised data.

ACKNOWLEDGMENT

We thank the team operating the JAEA tandem accelerator for providing the heavy-ion beams used in the experiment.

[1] A. V. Afanasjev, D. B. Fossan, G. J. Lane, and I. Ragnarsson, Phys. Rep. **322**, 1 (1999).
[2] J. Gizon, B. M. Nyakó, J. Timár, A. Gizon, L. Zolnai, A. J. Boston, G. Căta-Danil, J. Genevey, D. T. Joss, N. J. O'Brien *et al.*, Phys. Lett. B **410**, 95 (1997).
[3] D. Sohler, J. Timár, Z. Dombrádi, J. Cederkäll, J. Huijnen, M. Lipoglavšek, M. Palacz, A. Atac, C. Fahlander, H. Grawe *et al.*, Nucl. Phys. A **733**, 37 (2004).
[4] J. Timár, J. Gizon, A. Gizon, D. Sohler, B. M. Nyakó, L. Zolnai, A. J. Boston, D. T. Joss, E. S. Paul, A. T. Semple *et al.*, Phys. Rev. C **62**, 044317 (2000).
[5] J. Timár, J. Gizon, A. Gizon, L. Zolnai, B. M. Nyakó, G. Căta-Danil, D. Bucurescu, A. J. Boston, D. T. Joss, E. S. Paul *et al.*, Eur. Phys. J. A **4**, 11 (1999).
[6] M. E. Phelps and D. G. Sarantites, Nucl. Phys. A **135**, 116 (1969).
[7] G. Kajrys, G. Dufour, S. Pilotte, and S. Monaro, Phys. Rev. C **30**, 831 (1984).
[8] V. R. Kumar, V. Lakshminarayana, B. V. T. Rao, M. L. N. Raju, T. S. Reddy, S. Lakshminarayana, K. L. Narasimham, K. Premachand, B. M. Rao, and R. K. Bhowmik, J. Phys. G: Nucl. Part. Phys. **20**, 441 (1994).
[9] R. P. Singh, R. K. Bhowmik, S. S. Ghugre, and S. B. Patel, Eur. Phys. J. A **7**, 35 (2000).
[10] J. Timár, J. Gizon, A. Gizon, D. Sohler, B. M. Nyakó, L. Zolnai, G. Căta-Danil, D. Bucurescu, A. J. Boston, D. T. Joss *et al.*, Nucl. Phys. A **696**, 241 (2001).
[11] M. Sugawara, T. Hayakawa, M. Oshima, Y. Toh, A. Osa, M. Matsuda, T. Shizuma, Y. Hatsukawa, H. Kusakari, T. Morikawa *et al.*, Phys. Rev. C **86**, 034326 (2012).
[12] K. Furuno, M. Oshima, T. Komatsubara, K. Furutaka, T.Hayakawa, M. Kidera, Y. Hatsukawa, M. Matsuda, S. Mitarai, T. Shizuma *et al.*, Nucl. Instrum. Methods Phys. Res., Sect. A **421**, 211 (1999).
[13] D. C. Radford, Nucl. Instrum. Methods Phys. Res., Sect. A **361**, 297 (1995).

[14] M. Piiparinen, A. Ataç, J. Blomqvist, G. B. Hagemann, B. Herskind, R. Julin, S. Juutinen, A. Lampinen, J. Nyberg, G. Sletten *et al.*, Nucl. Phys. A **605**, 191 (1996).
[15] A. Charvet, R. Duffait, R. Beraud, K. Deneffe, A. Emsallem, M. Meyer, J. Treherne, and A. Gizon, Z. Phys. A **315**, 163 (1984).
[16] H. Dejbakhsh, R. P. Schmitt, and G. Mouchaty, Phys. Rev. C **37**, 621 (1988).
[17] S. S. Ghugre, B. Kharraja,, U. Garg, R. V. F. Janssens, M. P. Carpenter, B. Crowell, T. L. K. T. Lauritsen, D. Nisius, W. Reviol *et al.*, Phys. Rev. C **61**, 024302 (1999).
[18] D. Hippe, H. W. Schuh, U. Kaup, K. O. Zell, P. von Brentano, and D. B. Fossan, Z. Phys. A **311**, 329 (1983).
[19] K. O. Zell, H. Harter, D. Hippe, H. W. Schuh, and P. von Brentano, Z. Phys. A **316**, 351 (1984).
[20] P. H. Regan, C. W. Beausang, N. V. Zamfir, R. F. Casten, J. ye Zhang, A. D. Yamamoto, M. A. Caprio, G. Gürdal, A. A. Hecht, C. Hutter *et al.*, Phys. Rev. Lett. **90**, 152502 (2003).
[21] D. Bucurescu, A. Gadea, G. Căta-Danil, I. Căta-Danil, M. Ivaşcu, N. Mărginean, C. Rusu, L. Stroe, and C. A. Ur, Eur. Phys. J. A **16**, 469 (2003).